Numerical Simulation of Heat Transfer and Pressure Drop in Plate Heat Exchangers using FLUENT as a CFD Tool
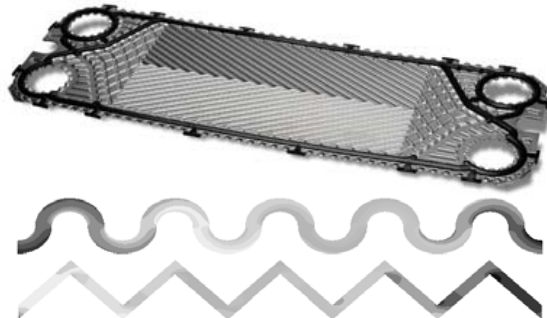
Dafe Egeregor

Department of Mechanical Engineering

Blekinge Institute of Technology

Karlskrona, Sweden

2008

Supervisors: Ansel Berghuvud, Ph.D Mech Eng, BTH
Joachim Claesson, Ph.D, Dept. of Energy Technology, KTH

NUMERICAL SIMULATION OF HEAT TRANSFER AND PRESSURE DROP IN PLATE HEAT EXCHANGERS USING FLUENT AS CFD TOOL

DAFE EGEREGOR

Department of Mechanical Engineering
Blekinge Institute of Technology
Karlskrona, Sweden
2008

Thesis submitted for the completion of Master of Science in Mechanical Engineering with emphasis on Structural Mechanics at the Department of Mechanical Engineering, Blekinge Institute of Technology, Karlskrona, Sweden.

Abstract

Corrugated walls are commonly used as passive devices for heat and mass transfer enhancement, being most effective in applications operated at transitional and turbulent Reynolds numbers. The plate heat exchanger (PHE) is an example of this application. In this thesis work, numerical simulation is used to investigate the heat transfer and pressure drop in plate heat exchangers, with the intention of determining the effect of channel geometry and flow conditions on the heat transfer of the exchangers. In this work two PHEs, one with a wave geometry, and one with a 'chevron' design was studied using Fluent as the CFD tool and Gambit as the preprocessor. In both cases, the temperature of the wall was kept constant, water was used as the working fluid, and the mass flow rate varied to study the effect of Reynolds number. The Reynolds number range simulated is 100-25,600.

Acknowledgement

Contents

Notations

English symbols

A	Area
A_n, B_n	Coefficients in Churchill's equation
c_p	Specific heat at constant pressure
C_{ijk}	Turbulent transport tensor
D	Pipe diameter
f	Friction factor
g	Acceleration due to gravity
h_f	Head loss
h	Convective heat transfer coefficient
k	Kinetic energy of turbulent fluctuations per unit mass
K_{fluid}	Thermal conductivity
ℓ_{mix}	Mixing length
L	Characteristic length scale
m	Mass-flow rate
Nu	Nusselt number
$N(u_i)$	Navier-Stokes operator
p	Instantaneous static pressure
q_{cond}	Conductive heat flux
q_{conv}	Convective heat flux
Q	Energy transfer
Re	Reynolds number
S_{ij}	Mean strain-rate tensor
t	Time
T	Temperature
T_i, T_o	Temperature at inlet and outlet of region under study
T_s	Surface temperature
T_w	Wall temperature
T_∞	Fluid temperature
u_i	Instantaneous velocity in tensor notation
u', v', w'	Fluctuating velocity components in x, y, z directions
u_i'	Fluctuating velocity in tensor notation
$\overline{u_i' u_j'}$	Temporal average of fluctuating velocities
U	Mean velocity component
U_i	Mean velocity in tensor notation

v_{mix}	Mixing velocity
v	Velocity
x_i	Position vector in tensor notation

Greek symbols

δ_{ij}	Kronecker delta
ε	Dissipation per unit mass
ε_{ij}	Dissipation tensor
ς	Absolute internal pipe roughness
μ	Molecular viscosity
ν	Kinematic molecular viscosity, μ/ρ
ν_T	Kinematic eddy viscosity, μ_T/ρ
Π_{ij}	Pressure-strain correlation tensor
ρ	Mass density
$\sigma(x)$	Non-equilibrium parameter
τ	Kolmogorov time scale; turbulence dissipation time
τ_{ij}	Specific Reynolds stress tensor, $-\overline{u_i' u_j'}$
ω	Specific dissipation rate; vorticity-vector magnitude

2. Introduction

Enhancement of heat transfer surfaces has developed over the years, and is the main focus in the heat exchanger industry. Enhanced surfaces yield higher heat transfer coefficient when compared to un-enhanced surfaces. A surface can basically be enhanced in two ways, either active enhancement which requires deployment of external power which is obviously high in operational and capital cost thus commercially unviable, and passive enhancement which involves adding extended surfaces (e.g. fins), or employing interrupted surfaces (e.g. corrugations).

The plate heat exchanger is widely recognized today as the most economical and efficient type of heat exchanger on the market. With it's low cost, flexibility, easy maintenance, and high thermal efficiency, it is unmatched by any type of heat exchanger. The key to the plate heat exchanger's efficiency lies in it's plates. With corrugation patterns that induce turbulent flows, it not only achieves unmatched efficiency, it also creates a self-cleaning effect thereby reducing fouling [1]. The most common surface pattern used is the chevron design.
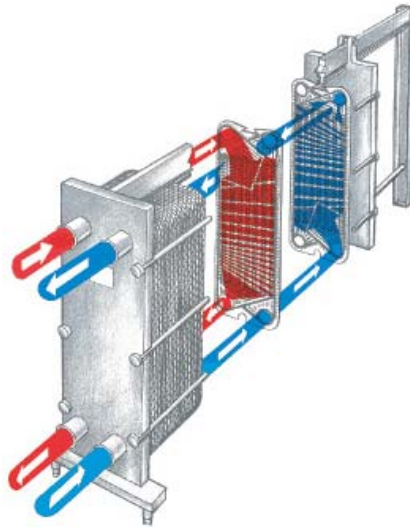
Fig 2.1 Heat exchanger plate

Plate heat exchangers are usually designed to achieve turbulence across the entire heat transfer area in order to get the highest possible heat transfer coefficient with the lowest possible pressure drop, and allow for close temperature approach. Consequently this means smaller heat transfer area, smaller heat exchangers, and sometimes even less heat exchangers [1].

The plate heat exchanger consists of a number of gasketed plates which are fixed between a top carrying bar and a lower guide bar. The plates are compressed by means of tie bolts between a stationary frame part (called the head), and a moveable frame part (called the follower) [1].

Fig 2.2 A plate heat exchanger

The plate heat exchanger is designed with either single-pass or multi-pass flow, depending on the application. For most applications, the single-pass solution is suitable and preferred because it keeps all connections on the stationary frame part and thus makes disassembly easier. However, for applications with low flow rates or close approach temperatures, the multi-pass solution is required [1].

Some of the advantages of the plate heat exchanger are discussed below [1];

- **Expandable:** the expandability of the plate heat exchanger is one of its significant features. Increasing the heat transfer requirement simply means adding plates instead of buying a new heat exchanger, thus saving time and money.
- **High efficiency:** due to the plate patterns and relatively narrow gaps, very high turbulence is achieved at relatively low fluid velocity. This combined with counter directional flow results in very high heat transfer coefficient.
- **Compact size:** consequent to it's high efficiency, a much smaller heat exchanger than would be needed for the same duty using other heat exchangers is obtained. Typically, a plate heat exchanger requires between 20-40% of the space requirement for a tube and shell heat exchanger.
- **Multiple duties in a single unit:** the plate heat exchanger can be built in sections separated with simple divider plates or more complicated divider frames with additional connections. This makes it possible to heat, regenerate, and cool a fluid in one heat exchanger, or heat or cool multiple fluids with the same cooling or heating source.
- **Less fouling:** the very high turbulence achieved as a result of the plate pattern and narrow gap, combined with the smooth plate surface reduces fouling considerably in comparison to other heat exchanger types.

- **Easy to remove and clean:** this is done by simply removing the tie bolts and sliding the movable frame part back. The plates can then be inspected, pressure cleaned, or removed for refurbishment if required.

To better understand the mechanisms of plate heat exchangers; their flow patterns, swirl flows, and effects on heat transfer and pressure drop, and to translate this into the development of new products, the numerical simulation of various design parameters is essential.

In the numerical simulation of plate heat exchangers, some assumptions are made, most of which do not correspond to real plate heat exchanger conditions. For example, the constant wall temperature/heat flux thermal boundary condition commonly specified does not correspond to real situation as the temperature and heat flux varies along the plate due to complex 3D flow caused by the shape of the corrugation pattern. For large plate heat exchangers, a fully developed flow approximation in the central region may be assumed, which is invalid for small plate heat exchangers because at the central region of the plate, the flow is still developing. Also, this developing region is not negligible when compared to the fully developed region [2].

To obtain an approximation of the actual results, the smallest geometry that simulates the heat exchanger would be analyzed.

For this thesis work, a 2D steady state analysis was carried out using GAMBIT as the preprocessor for geometry and mesh generation, and FLUENT 5/6 as the CFD tool for solving and post-processing. The inputs to the simulation include, the inlet mass-flow rate, inlet temperature, wall temperature, with liquid water as the working fluid. The simulation predicts the velocity, pressure and temperature distribution in the channel, and from these results, the heat transfer coefficient, Nusselt number and friction factor were calculated.

2.1 Literature review

As earlier mentioned, the enhancement of heat transfer surfaces has developed over the years, and several studies have been made in this area. During the course of this thesis, references were made to some of these studies to get an understanding of the task ahead. A brief review of these studies is introduced here.

First, a look at the study carried out by [2] titled 'A New Approach to Numerical Simulation of Small Sized Plate Heat Exchangers with Chevron Plates'. A numerical and experimental study of heat transfer and fluid flow in a single pass counter flow plate heat exchanger with chevron plates was presented. CFD analysis of small sized plate heat exchanger was carried out by taking the complete geometry of the heat transfer surface and more realistic hydrodynamic and thermal boundary conditions. A cold channel with two chevron plates and two halves of hot channel on either side having flat periodic boundaries was selected as the computational domain. Heat transfer and pressure drop data were obtained experimentally with water as the working fluid; in the Reynolds number range 400-1300 and Prandtl number range 4.4-6.3. The work considered a cold channel (with two corrugated plates on either side) and two half hot channels on either side as the computational domain. The virtual flat boundaries of the outer half hot channel were treated as periodic surfaces to represent the complete heat exchanger. In applying the periodic boundary conditions, the pack was assumed to contain infinite

plates (neglecting the end effects), although the end effects may be significant if the number of plates is less than 50 [3]. For the selected geometry, 3-D, steady state numerical simulations were carried out using GAMBIT as the preprocessor for geometry creation and mesh generation and FLUENT 5/6 as the solver and postprocessor. The inputs to the simulation included the inlet velocities and temperatures of hot and cold fluids. The simulations predicted the heat transfer coefficient and pressure drop along with the velocity, pressure, and temperature distribution in the channels. The realizable $k - \varepsilon$ turbulence model with non-equilibrium wall function was used.

An experimental study of heat transfer of corrugated channels, [4] was also consulted. This experimental study investigated the heat transfer characteristics of the corrugated channels in plate heat exchangers. A flow channel with wavy surfaces was constructed within which air was passed thru. The temperature of the wall was maintained constant. Starting from the entrance, the air temperatures within two wavelengths were measured at about 300 locations. The Reynolds number of air was varied from 300-9000. Results show that both the average and local Nusselt number decreases with the distance from the entrance and is greater at sections near the crest.

3. Mathematical Model

3.1 The turbulence energy equation

The development of turbulence energy equation models has incorporated non-local and flow history effects in the eddy viscosity. Prandtl (1945) postulated computing a characteristic velocity scale for the turbulence, υ_{mix}, thus rendering unnecessary the assumption $\upsilon_{mix} \approx \ell_{mix} |\partial U / \partial y|$. He chose the kinetic energy (per unit mass) of the turbulent fluctuations, k, as the basis of his velocity scale [5], i.e.,

$$k = \frac{1}{2}\overline{u_i^{'} u_i^{'}} = \frac{1}{2}\left(\overline{u^{'2}} + \overline{v^{'2}} + \overline{w^{'2}}\right) \tag{3.1}$$

Thus, the kinetic eddy viscosity in terms of k and the turbulent length scale, ℓ, by dimensional arguments is

$$v_T = \text{Constant} \cdot k^{1/2} \ell \tag{3.2}$$

The Reynolds-stress equation in suitable compact form [5] is given as;

$$\frac{\partial \tau_{ij}}{\partial t} + U_k \frac{\partial \tau_{ij}}{\partial x_k} = -\tau_{ik} \frac{\partial U_j}{\partial x_k} - \tau_{jk} \frac{\partial U_i}{\partial x_k} + \varepsilon_{ij} - \Pi_{ij} + \frac{\partial}{\partial x_k}\left[v \frac{\partial \tau_{ij}}{\partial x_k} + C_{ijk} \right] \tag{3.3}$$

Where

$$\Pi_{ij} = \overline{\frac{p^{'}}{\rho}\left(\frac{\partial u_i^{'}}{\partial x_j} + \frac{\partial u_j^{'}}{\partial x_i} \right)} \tag{3.4}$$

$$\varepsilon_{ij} = 2v\overline{\frac{\partial u_i^{'}}{\partial x_k} \frac{\partial u_j^{'}}{\partial x_k}} \tag{3.5}$$

$$\rho C_{ijk} = \overline{\rho u_i^{'} u_j^{'} u_k^{'}} + \overline{p^{'} u_i^{'}} \delta_{jk} + \overline{p^{'} u_j^{'}} \delta_{ik} \tag{3.6}$$

k can be determined by taking the trace of the Reynolds-stress tensor, which yields [5];

$$\tau_{ii} = -\overline{u_i^{'} u_i^{'}} = -2k \tag{3.7}$$

A corresponding equation for k can be derived by taking the trace of the Reynolds-stress equation (3.3). Note that for incompressible flow, the trace of the tensor Π_{ij} vanishes, thus obtaining the transport equation for the turbulence kinetic energy [5];

$$\frac{\partial k}{\partial t} + U_j \frac{\partial k}{\partial x_j} = \tau_{ij} \frac{\partial U_i}{\partial x_j} - \varepsilon + \frac{\partial}{\partial x_j}\left[v\frac{\partial k}{\partial x_j} - \frac{1}{2}\overline{u_i' u_i' u_j'} - \frac{1}{\rho}\overline{p' u_j'} \right] \qquad (3.8)$$

$$\varepsilon = v\overline{\frac{\partial u_i'}{\partial x_k} \frac{\partial u_i'}{\partial x_k}} \qquad (3.9)$$

The terms appearing in equation (3.8) represent the physical processes occurring as turbulence moves about a given flow. The sum of the two terms on the left-hand side, i.e., the unsteady term and the convection, is the familiar substantial derivative of k that gives the rate of change of k following a fluid particle. The first term on the right-hand side is known as production, and represents the rate at which kinetic energy is transferred from the mean flow to the turbulence. Rewritten as $\tau_{ij} S_{ij}$ (because τ_{ij} is symmetric), this term is seen to be the rate at which work is done by the mean strain rate against the turbulent stresses. Dissipation is the rate at which turbulence kinetic energy is converted into thermal internal energy, equal to the mean rate at which work is done by the fluctuating part of the strain rate against the fluctuating viscous stresses. The term involving $v\dfrac{\partial k}{\partial x_j}$ is called molecular diffusion, and represents the diffusion of turbulence energy caused by the fluid's natural molecular transport process. The triple velocity correlation term is referred to as turbulent transport, and is regarded as the rate at which turbulence energy is transported through the fluid by turbulent fluctuations. The last term on the right-hand side of the equation is called the pressure diffusion, another form of turbulent transport resulting from correlation of pressure and velocity fluctuations [5].

The unsteady term, convection and molecular diffusion are exact while production, dissipation, turbulent transport and pressure diffusion involve unknown correlations. To close this equation, we must specify τ_{ij}, dissipation, turbulent transport and pressure diffusion [5].

The conventional approach to closure of the k equation was initiated by Prandtl (1945) who established arguments for each term in the equation. This term-by-term modeling approach amounts to performing drastic surgery on the exact equation, replacing unknown correlations with closure approximations [5].

This closure gives the following approximations [5];

$$\tau_{ij} = 2v_T S_{ij} - \frac{2}{3}k\delta_{ij} \qquad (3.10)$$

This equation, (3.10) is known as the Boussinesq approximation.

$$\frac{1}{2}\overline{u_i' u_i' u_j'} + \frac{1}{\rho}\overline{p' u_j'} = -\frac{v_T}{\sigma_k}\frac{\partial k}{\partial x_j} \qquad (3.11)$$

Combining equations (3.8) and (3.11) gives the modeled version of the turbulence kinetic energy equation used in virtually all turbulence energy equation models. The equation is of the form [5];

$$\frac{\partial k}{\partial t} + U_j \frac{\partial k}{\partial x_j} = \tau_{ij} \frac{\partial U_i}{\partial x_j} - \varepsilon + \frac{\partial}{\partial x_j}\left[\left(v + \frac{v_T}{\sigma_k}\right)\frac{\partial k}{\partial x_j}\right] \tag{3.12}$$

3.2 Two-equation models

Two-equation models provide not only for the computation of k, but also for the computation of the turbulence length scale or its equivalent. Two-equation models are complete, i.e., they can be used to predict properties of a given turbulent flow without prior knowledge of the turbulence structure.

The turbulence kinetic energy equation and the Boussinesq approximation are the starting point for all two-equation models. There is arbitrariness in the way the turbulence length scale is defined in relation to the velocity scale. [6] pointed out that a second transport equation is needed to compute the specific dissipation rate, ω. This quantity has dimensions of $(time)^{-1}$. The eddy viscosity, turbulence length scale and dissipation can be determined on dimensional arguments from [5];

$$v_T \approx \frac{k}{\omega}, \qquad \ell \approx \frac{k^{1/2}}{\omega}, \qquad \varepsilon \approx \omega k \tag{3.13}$$

[7] proposed modeling the exact equation for ε. In terms of this formulation, the kinematic eddy viscosity and turbulence length scale are [5];

$$v_T \approx \frac{k^2}{\varepsilon}, \qquad \ell \approx \frac{k^{3/2}}{\varepsilon} \tag{3.14}$$

[8] proposed an equation for the product of k and ℓ [5];

$$v_T \approx k^{1/2}\ell, \qquad \varepsilon \approx \frac{k^{3/2}}{\ell} \tag{3.15}$$

[9] introduced a transport equation for the product of k and turbulence dissipation time, τ. [10] postulated an equation for τ [5];

$$v_T \approx k\tau, \qquad \ell \approx k^{1/2}\tau, \qquad \varepsilon \approx \frac{k}{\tau} \tag{3.16}$$

On the basis of dimensional arguments, the choice of the second variable is of no consequence as the dissipation, eddy viscosity and length scale are all related. It should be noted here that while dimensional analysis is extremely useful, it reveals nothing about the physics underlying its implied scaling relationships. The physics is in the choice of variables [5].

3.2.1 The $k - \varepsilon$ model

No single turbulence model is best for all cases of problems. Fluent, the CFD tool for this thesis work provides a number of choices which include the standard, RNG (renormalization group), and realizable $k - \varepsilon$ models, the standard and SST (shear stress transport) $k - \omega$ models, the Reynolds stress model (RSM), and the large eddy simulation (LES) model. The appropriate choice of a turbulence model would be, striking a balance between the physics of the flow, level of accuracy, established practices, available computational resources, etc.

Different researchers have reported the use of different turbulence models for studies on plate heat exchangers. The choice of the $k - \varepsilon$ model is natural, I thinking, being the far most popular two-equation model. However, the choice of the realizable model is by recommendation by Fluent, as it provides the best performance of all the $k - \varepsilon$ model versions for several validations of separated flows and flows with complex secondary flow features [11].

The earliest development efforts on the $k - \varepsilon$ model were those of [7], [12], and [13]. However, the widespread use of the model began with the introduction of the [14] version, whose closure coefficients were subsequently 'retuned' by [15] to produce the standard $k - \varepsilon$ model [5].

The idea behind formulating the $k - \varepsilon$ model is to derive the exact equation for ε and find suitable closure approximations for the exact equation governing it's behaviour. The exact equation for ε is derived by taking the moment of the Navier-Stokes equation [5];

$$2v\overline{\frac{\partial u_i^{'}}{\partial x_j}\frac{\partial}{\partial x_j}\left[N(u_i)\right]} = 0 \tag{3.17}$$

Where

$$N(u_i) = \rho\frac{\partial u_i}{\partial t} + \rho u_k\frac{\partial u_i}{\partial x_k} + \frac{\partial p}{\partial x_i} - \mu\frac{\partial^2 u_i}{\partial x_k\partial x_k} \tag{3.18}$$

The following exact equation for ε is obtained after a considerable amount of algebra [5];

$$\frac{\partial\varepsilon}{\partial t} + U_j\frac{\partial\varepsilon}{\partial x_j} = -2v\left[\overline{u_{i,k}u_{j,k}}^{,'} + \overline{u_{k,i}u_{k,j}}^{,'}\right]\frac{\partial U_i}{\partial x_j} - 2v\overline{u_k u_{i,j}}^{,'}\frac{\partial^2 U_i}{\partial x_k\partial x_j} - 2v\overline{u_{i,k}u_{i,m}u_{k,m}}^{,'}$$
$$- 2v^2\overline{u_{i,km}u_{i,km}}^{,'} + \frac{\partial}{\partial x_j}\left[v\frac{\partial\varepsilon}{\partial x_j} - v\overline{u_j u_{i,m}u_{i,m}}^{,'} - 2\frac{v}{\rho}\overline{p_{,m}u_{j,m}}^{,'}\right] \tag{3.19}$$

This equation is far more complicated than the turbulent kinetic energy equation and involves several unknown double and triple correlations of fluctuating velocity, pressure and velocity gradients. DNS studies [16] provide some insight into the exact ε equation for low Reynolds number flows. The database for establishing the closure approximations similar to those of the k equation remains very sparse. The strongest claim that can be made however is that, the conventional closure approximations used for equation (3.19) are dimensionally correct [5].

It is important to avoid modeling the differential equation rather than the physics of turbulence. This doesn't mean avoiding any reference to the differential equations, unless a model that violates the fundamental physical features of the Navier-Stokes equation might result [5].

The standard $k - \varepsilon$ model is thus given [5];

Kinetic eddy viscosity:

$$v_T = C_\mu \frac{k^2}{\varepsilon} \tag{3.20}$$

Turbulence kinetic energy:

$$\frac{\partial k}{\partial t} + U_j \frac{\partial k}{\partial x_j} = \tau_{ij} \frac{\partial U_i}{\partial x_j} - \varepsilon + \frac{\partial}{\partial x_j}\left[\left(v + \frac{v_T}{\sigma_k}\right)\frac{\partial k}{\partial x_j}\right] \tag{3.21}$$

Dissipation rate:

$$\frac{\partial \varepsilon}{\partial t} + U_j \frac{\partial \varepsilon}{\partial x_j} = C_{\varepsilon 1} \frac{\varepsilon}{k} \tau_{ij} \frac{\partial U_i}{\partial x_j} - C_{\varepsilon 2} \frac{\varepsilon^2}{k} + \frac{\partial}{\partial x_j}\left[\left(v + \frac{v_T}{\sigma_\varepsilon}\right)\frac{\partial \varepsilon}{\partial x_j}\right] \tag{3.22}$$

Closure coefficients and auxiliary relations:

Table 3.1 Closure coefficients and auxiliary relations

$C_{\varepsilon 1}$	$C_{\varepsilon 2}$	C_μ	σ_k	σ_ε	ω	ℓ
1.44	1.92	0.09	1.0	1.3	$\varepsilon/(C_\mu k)$	$C_\mu k^{3/2}/\varepsilon$

4. Solution Methodology

4.1 Geometry generation and meshing

As earlier mentioned, the analysis was carried out using Gambit as the preprocessor for the geometry creation and mesh generation. The geometry was created with the 'Tools' operations, using the 'display grid' under the 'coordinate system'. A minimum value of -15, a maximum value of 15, and an increment value of 1 were specified along the x-axis. Along the y-axis, a minimum value of -2, a maximum value of 2, and an increment value of 1 was specified. The geometry was then created.

The next step was defining the grid density on the boundary edges of the geometry and meshing.

Table 4.1 Geometry boundary edge grid specification

Boundary	Specification
Inlet	Successive ratio, ratio value of 1.11, double sided, interval count, and spacing of 15
Outlet	Successive ratio, ratio value of 1.11, double sided, interval count, and spacing of 15
Wall edges	Successive ratio, ratio value of 1, interval count, and spacing of 60

The final step here is specifying the boundary types, which are, inlet (mass-flow-rate), and outlet (outflow).

The exact same procedure is used for the chevron design as appropriate.

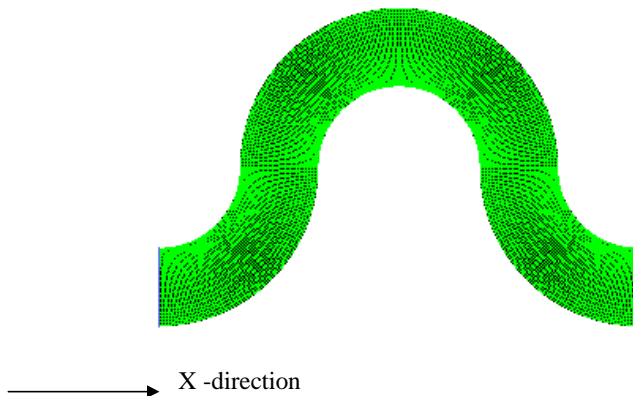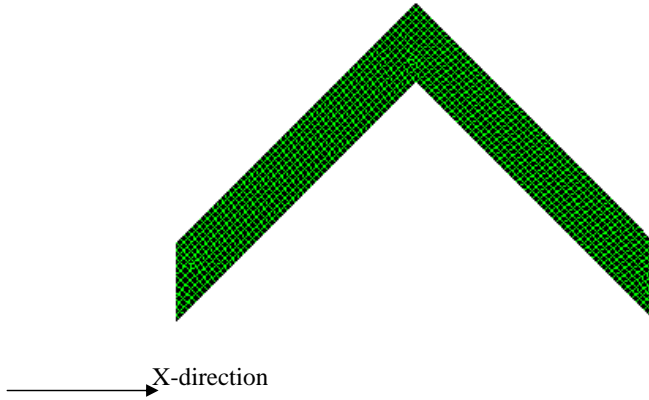*Fig 4.1 Cross-section of wave geometry considered*

X -direction

Fig 4.2 Cross-section of chevron geometry considered

X-direction

4.2 Analysis and solution

The governing equations were solved using the commercial CFD package FLUENT 5/6 with the following simplifying assumptions [2]:

1. Being a small PHE, there is no mal-distribution of flow.
2. Heat transfer surface assumed to be free from fouling.
3. Periodicity exists in the X-direction.

The following settings were used for the model solution

Table 4.2 (a) & (b) Simulation settings

Function	Specification
Solver	Default: segregated (solver), implicit (formulation), 2D (space), absolute (velocity formulation), cell based (gradient orientation), superficial velocity (porous formulation)
Energy	Enable energy equation
Viscous	Laminar: laminar Turbulent: $k - \varepsilon$, realizable, non-equilibrium wall function. Every other setting is default; $C_{\varepsilon 2} = 1.9$, $\mathrm{Pr}_k = 1.0$, $\mathrm{Pr}_\varepsilon = 1.2$, $\mathrm{Pr}_T = 0.85$, $\mathrm{Pr}_\omega = 0.85$
Material	Water-liquid. Default: $\rho = 998.2\,Kg/m^3$, $C_p = 4182\,J/kgK$, $k = 0.6\,w/mK$, $\mu = 0.001003\,Kg/ms$

(a)

Function	Specification
Boundary conditions: Fluid	Water-liquid. Every other thing is default.
Inlet	Mass flow rate (Mass flow rate specification method), Mass-flow rate = 0.05015Kg/s (one of the values used), Total temperature = 315K, Supersonic/initial gauge pressure = 0Pa, Direction vector (Direction specification method), Absolute (Reference frame), X-component of flow direction = 1, Y-component of flow direction = 0, Intensity and hydraulic diameter (Turbulence specification method), Turbulence intensity = 5%, Hydraulic diameter = 0.02
Outlet	Default: Flow-rate weighting=1
Wall	Thermal: Temperature (Thermal conditions), Temperature = 350K, Wall thickness = 0m, Heat generation rate $= 0 \, w/m^3$, Aluminum (default; material name) Momentum: Stationary wall (Wall motion), No slip (shear condition), Roughness height = 0m, Roughness constant = 0.5
Solution controls	SIMPLE (Pressure-velocity coupling), Under-Relaxation factors: Pressure = 0.3, Density = 1, Body forces = 1, Momentum = 0.7, Turbulence kinetic energy = 0.8, Turbulence dissipation rate = 0.8, Turbulent viscosity = 1, Energy = 0.9. Discretization: PRESTO (Pressure), Second order upwind (Momentum, Turbulent kinetic energy, Turbulent dissipation rate, and Energy)
Residual monitors	Print and Plot (Options), Default: Convergence criterion; Continuity = 0.001, X-velocity = 0.001, Y-velocity = 0.001, Energy = 1e-06, k = 0.001, ε = 0.001. Scale (Normalization)
Solution initialization	Default: Relative to cell zone (Reference plane), Initial values: Gauge pressure = 0Pa, X-velocity = 0m/s, Y-velocity = 0m/s, Turbulent kinetic energy $= 1 \, m^2/s^2$, Turbulent dissipation rate $= 1 \, m^2/s^3$, Temperature = 300K

(b)

It is assumed that the flow is uniformly distributed at the entry of the heat transfer surface. The hydraulic diameter is specified as twice the mean flow channel gap.

Most of the choices made are based on previous studies on plate heat exchangers, especially the work done by [2], which infer/ state these to be the most appropriate settings for a $k - \varepsilon$ model, using FLUENT as CFD tool.

Note: After results were obtained, the mesh was refined and the solution recalculated, until a result that isn't mesh dependent was obtained. The mesh details are given below,

Wave design:
19216 nodes.
   2400 mixed wall faces, zone 3.
    15 mixed outflow faces, zone 4.
    15 mixed mass-flow-inlet faces, zone 5.
  34785 mixed interior faces, zone 7.
  18000 quadrilateral cells, zone 2.

Chevron design:
6490 nodes.
   1200 mixed wall faces, zone 3.
    15 mixed outflow faces, zone 4.
    15 mixed mass-flow-inlet faces, zone 5.
  11133 mixed interior faces, zone 7.
 5874 quadrilateral cells, zone 2.

5. Results and Discussion

Simulations were carried out with Reynolds numbers varying between 100 and 25,600. The post processing was carried out in FLUENT, and during the process, the following observations were encountered; for the simulation, 5 Reynolds numbers (100, 200, 400, 800, and 1600) corresponding to laminar flow and 4 Reynolds numbers (3200, 6400, 12800, and 25600) corresponding to turbulent flow were used. It was observed that when a laminar viscous model was specified for the laminar Reynolds numbers, only the 100 and 200 Reynolds numbers converged. The other 3 did not converge, and kept reporting reverse flow. However, when the turbulent $k - \varepsilon$ model was used, the solution converged.

This phenomenon could be attributed to the fact that most quantification/ criteria for determination of laminar or turbulent flows are carried out in straight pipes (the critical Reynolds number is approximately 2,300 and fully turbulent conditions occur at Reynolds number greater than 10,000. Between Reynolds number 2,300 and 10,000, the flow is considered to be in transition), but in the plate heat exchanger, as earlier mentioned, the corrugated patterns induce turbulent flow. So a mass flow rate which would naturally fall under laminar flow in a straight pipe might exhibit turbulent or transitional characteristics, and for the case in study, this takes place somewhere between 200 and 400 Reynolds numbers.

For a thermally fully developed flow of a fluid with constant properties, the local convection coefficient is a constant, independent of length. Iso-surfaces were created along the geometry far away from the inlet to ensure a fully developed flow (points 0.03m and 0.09m).

Fig 5.1 Cross section showing calculation domain
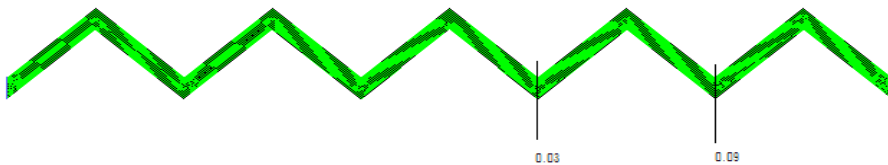
It is at these points that the results below, for a mass-weighted average were obtained.

Table 5.1 Simulated and calculated results for wave design

Re	$\dot{m}$	T_o	T_i	Δp (Ps)	V (m/s)	Nu	f
100	0.05015	335.64	332.64	0.07	0.0061	7.4510	0.0754
200	0.1003	328.74	326.45	0.15	0.0126	7.5871	0.0379
400	0.2006	344.62	341.41	0.95	0.021	69.4063	0.0863
800	0.4012	337.28	333.63	2.60	0.041	74.8411	0.0620
1600	0.8024	329.48	326.57	7.33	0.081	78.6858	0.0448
3200	1.6048	323.42	321.55	21.08	0.162	80.6799	0.0322
6400	3.2096	321.11	319.30	61.61	0.325	144.2199	0.0234
12,800	6.4192	320.04	318.60	197.99	0.655	222.8297	0.0185
25,600	12.8384	318.93	317.98	693.48	1.324	285.9184	0.0159

Table 5.2 Simulated and calculated results for chevron design

Re	$\overset{.}{m}$	T_o	T_i	Δp (Ps)	V (m/s)	Nu	f
100	0.05015	339.19	335.89	0.16	0.0092	7.7604	0.0536
200	0.1003	332.94	330.05	0.44	0.0197	9.1171	0.0321
400	0.2006	339.95	336.21	2.15	0.0294	36.8629	0.0705
800	0.4012	331.63	328.37	6.03	0.058	38.0693	0.0508
1600	0.8024	325.45	323.18	18.11	0.12	41.2174	0.0356
3200	1.6048	323.14	321.26	67.81	0.256	63.0611	0.0293
6400	3.2096	322.13	320.49	258.60	0.517	106.5968	0.0274
12,800	6.4192	321.55	320.02	1037.01	1.045	195.3114	0.0269
25,600	12.8384	321.13	319.65	4120.16	2.09	372.8090	0.0267

Recall that the inlet temperature is 315k and the wall temperature 350k. T_i and T_o represent the temperatures at the iso-surfaces.

Also, for reference purpose, the simulation for a straight pipe of the same length and diameter was carried out to compare the Nusselt number and friction factor values with that of the wavy and chevron design.

5.1 Nusselt number

The Nusselt number is an important dimensionless parameter that represents the temperature gradient at a surface where heat transfer by convection is taking place. It is a function of the Reynolds number, the Prandtl number, and if the fluid is still at the hydrodynamic entrance region, the Nusselt number will also vary as a function of the length of the tube. However, if the flow is fully developed, the Nusselt number becomes constant [17].

If the value of the Nusselt number is unity, then it is pure conduction. Higher values mean that heat transfer is enhanced by convection. A large Nusselt number means very efficient convection; for example, turbulent pipe flow yields a Nusselt number of order 100 to 1000.

The concept of Nusselt number would be explained taking a look at what happens in the boundary layer. When a fluid flows over a surface, the first layer of the fluid sticks to the boundary (No slip condition; specified above in the solution section). This causes the flow to retard in the vicinity of the wall. Moving away from the wall, the effect of this no slip gets smaller and smaller until a point where it is no longer felt by the fluid. The layer between the wall and this point is what is referred to as the boundary layer [18].

When for example a cold fluid flows over a hot surface, the first layer of the fluid (which is stuck to the surface) gets heat from the surface by pure conduction. It then gives this newly acquired energy to all of the fluid molecules that it comes in contact with as they pass by it (this is convection) [18].

For the no slip condition,

$$q_{cond} = -K_{fluid} \left[\frac{dT}{dy} \right]_{y=0}$$
(5.1)

This heat flux is what will be taken away through convection by the moving fluid;

$$q_{conv} = h(T_s - T_\infty)$$
(5.2)

But,

$$q_{cond} = q_{conv}$$
(5.3)

This implies,

$$h = K_{fluid} \frac{\left[\frac{dT}{dy} \right]_{y=0}}{(T_s - T_\infty)}$$
(5.4)

This gives a simple definition of the heat transfer coefficient. The dimension of h from equation (5.4) is K/L since the temperatures cancel out. Thus dividing equation (5.4) by K/L gives the Nusselt number.

$$Nu = \frac{hL}{K}$$
(5.5)

In terms of the boundary, the characteristic length is the thickness of the boundary layer. Consider a fluid layer of thickness L and a temperature difference of ΔT across this layer. Heat transfer by convection can be calculated as $h\Delta T$ and the heat transfer by conduction as $K\Delta T / L$ [18].

This implies,

$$\frac{q_{conv}}{q_{cond}} = \frac{h\Delta T}{K\Delta T / L} = \frac{hL}{K} = Nu$$
(5.6)

So the Nusselt number may be viewed as the ratio of convection to conduction for a layer of fluid. Considering the conditions in this study; since the fluid experiences a large change in temperature as it moves through the channel, the heat transfer rate could be significantly over-predicted by using $\Delta T = T_s - T_\infty$ as the temperature difference in Newton's law of cooling. As the fluid moves through the channel, it's temperature approaches T_s and $|\Delta T|$ decreases. The log mean temperature is thus the appropriate form of ΔT [19].

$$Lmtd = \frac{(T_w - T_i) - (T_w - T_o)}{\ln\left(\frac{T_w - T_i}{T_w - T_o}\right)}$$ (5.7)

Also, from equation (5.2), it implies

$$h = \frac{q}{Lmtd}$$ (5.8)

But,

$$q = \frac{Q}{A}$$ (5.9)

And,
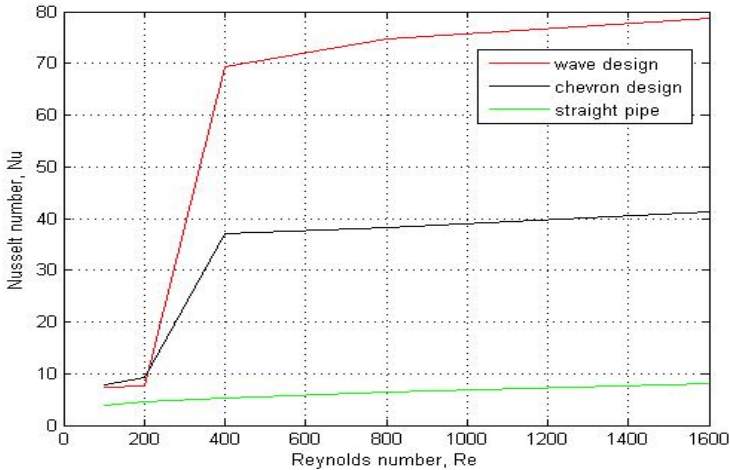
$$Q = mc_p \Delta T$$ (5.10)
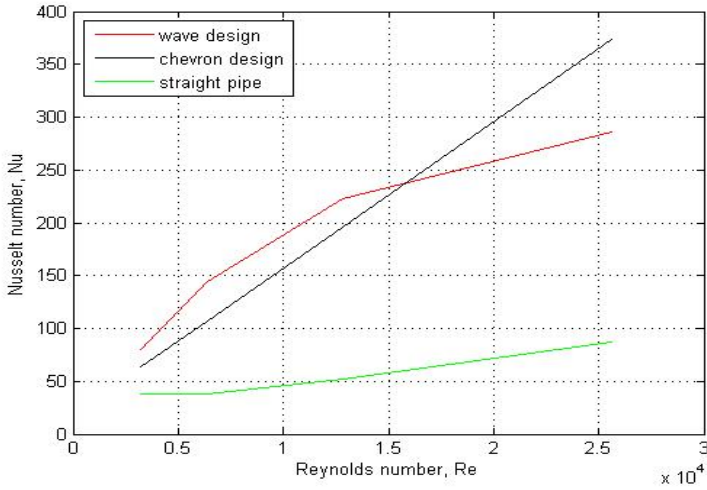
Thus,

$$h = \frac{mc_p \Delta T}{A \times Lmtd}$$ (5.11)

As can be seen from tables 5.1 and 5.2, Nusselt number increases with increase in the Reynolds number. The variation of the Nusselt number with Reynolds number is given below;

Figure 5.1 Variation of Nusselt number with Reynolds number: (a) laminar; (b) turbulent

(b)

From fig. 5.1 (a), the effect of using a turbulent model for a laminar Reynolds number flow can be seen by the sharp increase in the value of the Nusselt number, which is not present in the straight pipe. Also from fig. 5.1 (a) and (b), it can be observed that the chevron design gives a smoother transition when compared to the wave design. It shows a constant proportionality between the Nusselt and Reynolds numbers, unlike that of the wave design, which is probably why it is the most commonly used design.

At Reynolds number less than 16,000, fig. 5.1 (a) and (b) show higher values of Nusselt number for the wave design, while for higher Reynolds numbers, the chevron design gives higher values of Nusselt number

5.2 Friction factor

The head loss resulting from the flow of a fluid through a pipe is expressed by the Darcy equation;

$$h_f = f \frac{Lv^2}{2Dg} \tag{5.12}$$

The Hagen-Poiseulli equation for laminar flow indicates that the head loss is independent of surface roughness [20];

$$h_f = \frac{32\mu Lv}{\rho g D^2} \tag{5.13}$$

Comparing equations (5.7) and (5.8), it can be shown that;

23

$$f = \frac{64\mu}{\rho vD} = \frac{64}{\text{Re}} \tag{5.14}$$

Equation (5.14) shows that the friction factor is proportional to viscosity, and inversely proportional to velocity, pipe diameter, and the fluid density under laminar flow conditions. The friction factor is independent of the pipe roughness in lamina flow because the disturbances caused by surface roughness are quickly damped by viscosity.

When the flow is turbulent, the relationship becomes more complex and is best shown using a graph since the friction factor is a function of both Reynolds number and roughness. The relationship between friction factor and Reynolds number can be determined for every relative roughness. From these relationships, it is apparent that for rough pipes, the roughness is more important than the Reynolds number in determining the magnitude of the friction factor. At high Reynolds number (complete turbulence) for rough pipes, the friction factor depends entirely on roughness and the friction factor can be obtained from the rough pipe law [20];

$$\frac{1}{\sqrt{f}} = 2\log\left[\frac{3.7D}{\varsigma}\right] \tag{5.15}$$

For smooth pipes, the friction factor is independent of roughness and is given by the smooth pipe law;

$$\frac{1}{\sqrt{f}} = 2\log\left[\frac{\text{Re}\sqrt{f}}{2.51}\right] \tag{5.16}$$

The rough and smooth pipe laws were developed by Von Karman (1930). However, many pipe flow problems are in the 'transition zone', i.e. between the rough and smooth pipe law. In this zone, head loss is a function of both the Reynolds number and the pipe roughness. The friction factor is commonly computed via the implicit Colebrook-White (1939) equation. The Moody diagram is based on the Colebrook equation in the turbulent regime [20];

$$\frac{1}{\sqrt{f}} = -2\log\left[\frac{\varsigma}{3.7D} + \frac{2.51}{\text{Re}\sqrt{f}}\right] \tag{5.17}$$

More recently, the friction factor is computed explicitly by the Churchill equation, and by the Swanee-Jain equation.

Churchill equation:

$$f = 8\left[\left(\frac{8}{\text{Re}}\right)^{12} + \frac{1}{(A+B)^{3/2}}\right]^{1/12} \tag{5.18}$$

$$A_n = \left[2.457 \log_e \frac{1}{\left(\dfrac{7}{\text{Re}} \right)^{0.9} + \dfrac{0.27\varsigma}{D}} \right]^{16} \tag{5.19}$$

$$B_n = \left[\frac{37530}{\text{Re}} \right]^{16} \tag{5.20}$$

Swanee-Jain equation:

$$f = \frac{0.25}{\left[\log\left(\dfrac{\varsigma}{3.7D} + \dfrac{5.74}{\text{Re}^{0.9}} \right) \right]^2} \tag{5.21}$$

The Colebrook-White and Swanee-Jain equations were designed for the turbulent flow regime, but can also be used for the critical regime. Churchill's equation spans the entire range from laminar to turbulent.

The graph showing the variation of the Darcy friction factor with the Reynolds number is given below,

Figure 5.2 Variation of friction factor with Reynolds number: (a) laminar; (b) turbulent; (c) laminar log scale; (d) turbulent log scale
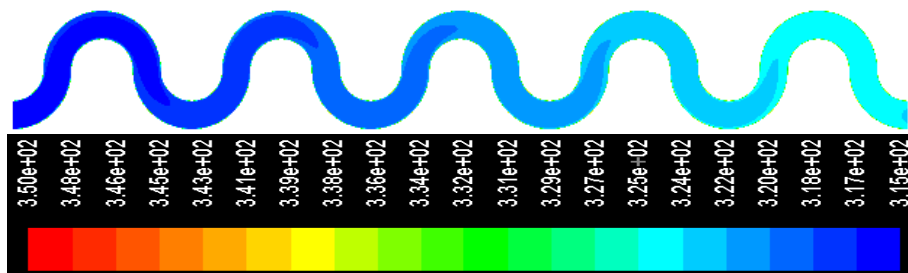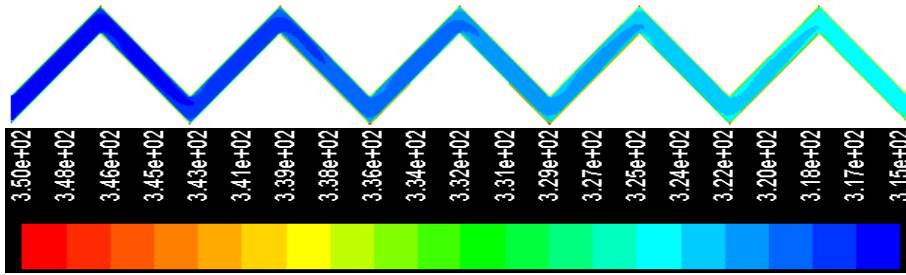

(a)

(b)

(c)

26

(d)
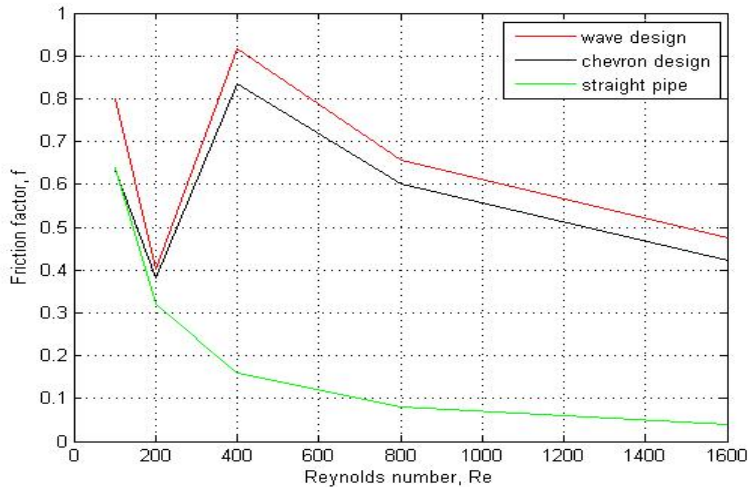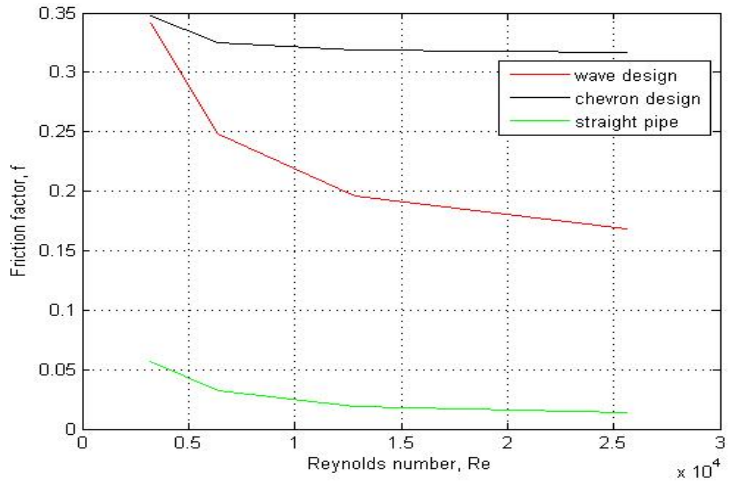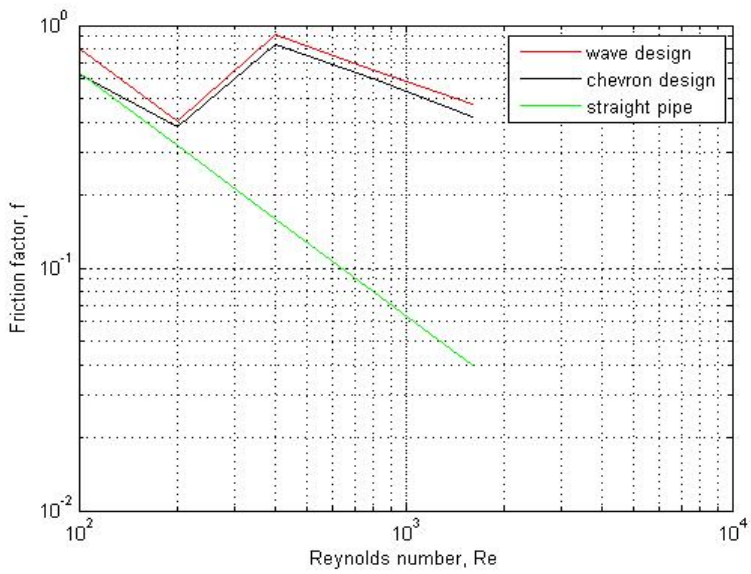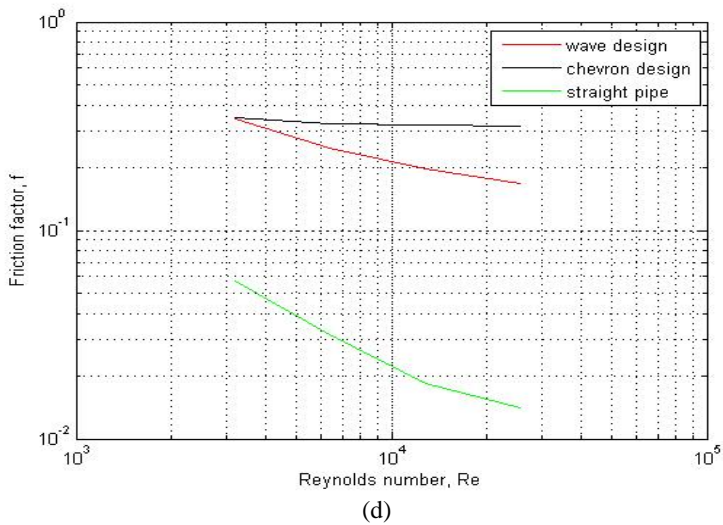
From fig. 5.2 (a) and (c), as in fig. 5.1 (a), the effect of using a turbulent model for a laminar Reynolds number flow is very visible. For the laminar region, the wave design gives higher friction factor values, and both geometries (wave and chevron) generally give the same variation pattern with the Reynolds number. However, from fig. 5.2 (b) and (d), the chevron design gives higher friction factor values, and has a very small slope which is almost a straight line. This shows that for high Reynolds numbers, there is almost no variation of the friction factor with the Reynolds number. This might also be the reason for the preference of the chevron design.

5.3 Temperature and velocity distribution

The mean temperature of the working fluid increases with the distance from the entrance as expected, as shown in fig. 5.3. Also expected, the increase is rapid nearer the entrance because of high heat transfer rates in this region due to higher temperature differences between the wall surface and the fluid. However, after the entrance region, the increase rate reduces gradually as shown in fig. 5.3.

Figure 5.3 Contours of static temperature at Re 3200: (a) wave design (b) chevron design

3.50e+02 3.48e+02 3.46e+02 3.45e+02 3.43e+02 3.41e+02 3.39e+02 3.38e+02 3.36e+02 3.34e+02 3.32e+02 3.31e+02 3.29e+02 3.27e+02 3.25e+02 3.24e+02 3.22e+02 3.20e+02 3.18e+02 3.17e+02 3.15e+02
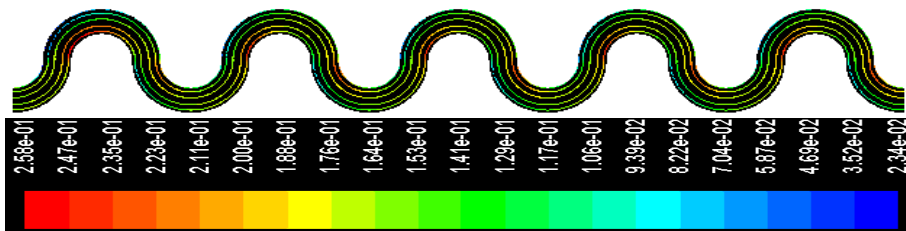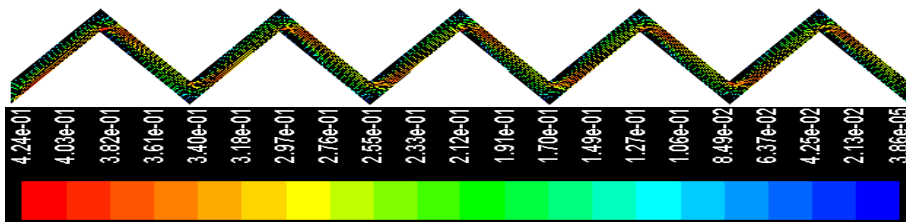
(b)

For a fully developed flow, the average velocity is constant and increases with increasing Reynolds number. From fig. 5.4, it is observed that the velocity profile is constant almost through the entire flow path, showing that the flow is fully developed. It can also be observed that the local velocity is highest at the curves in the flow direction.

Figure 5.4 Velocity vectors at Re 3200: (a) wave design (b) chevron design

2.58e-01 2.47e-01 2.35e-01 2.23e-01 2.11e-01 2.00e-01 1.88e-01 1.76e-01 1.64e-01 1.53e-01 1.41e-01 1.29e-01 1.17e-01 1.06e-01 9.39e-02 8.22e-02 7.04e-02 5.87e-02 4.69e-02 3.52e-02 2.34e-02

(a)

4.24e-01 4.03e-01 3.82e-01 3.61e-01 3.40e-01 3.18e-01 2.97e-01 2.76e-01 2.55e-01 2.33e-01 2.12e-01 1.91e-01 1.70e-01 1.49e-01 1.27e-01 1.06e-01 8.49e-02 6.37e-02 4.25e-02 2.13e-02 3.86e-05

(b)

Furthermore, the velocity profile at different points along the flow (iso-surface values) was simulated for different Reynolds numbers, one laminar, Re 200, and one turbulent, Re 3200, to show the variation of the velocity profile with the plate geometry.
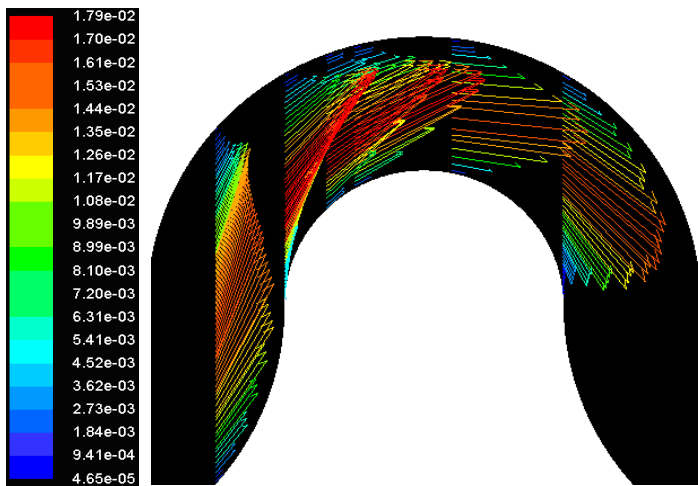
From fig. 5.5, it can be observed that for the wave design, as the flow moves towards the curve, particularly at the point of curvature of the inner curve, the velocity of the flow increases and the flow

28

separates. This happens both for the laminar and turbulent flow conditions. The velocity then drops in the curve and picks up again at the beginning of another curve.

Figure 5.5 Vector plot for velocity of wave design at iso-surface values 0.045, 0.05, 0.053, 0.055, 0.062, and 0.07 (a) at Re 3200 (b) at Re 200
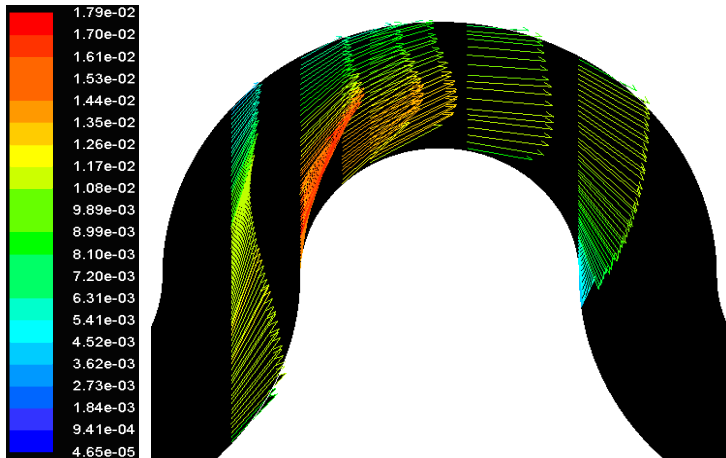

(a)

(b)

From fig. 5.6, it can be observed that for the chevron design, at every point where the flow direction changes, i.e. at the peaks, the flow velocity increases and the flow separates. Also from fig. 5.6, it can be seen that there is reverse flow for both the laminar and turbulent flow conditions.

Figure 5.6 Vector plot for velocity of chevron design at iso-surface values 0.045, 0.048, 0.055, 0.06, 0.062, and 0.065: (a) at Re 3200 (b) at Re 200
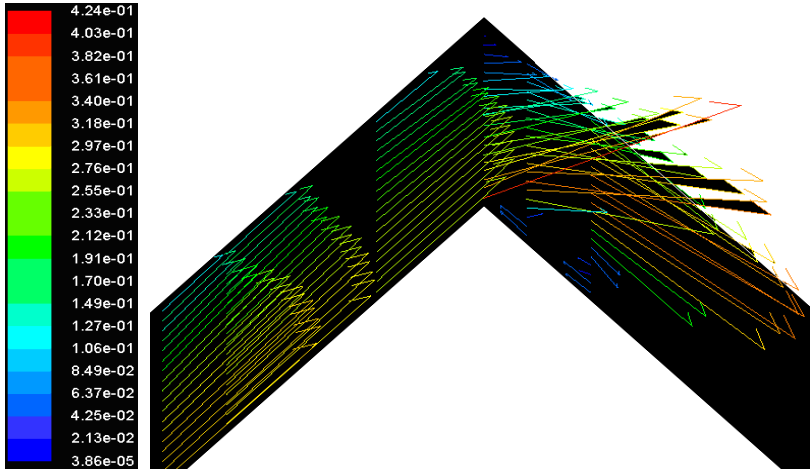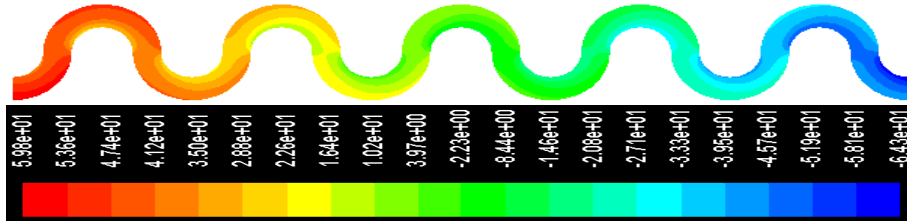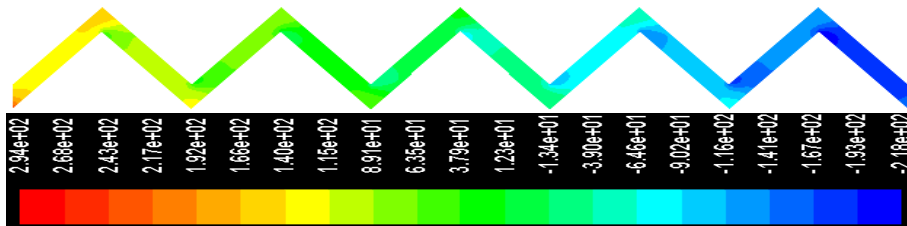

(a)
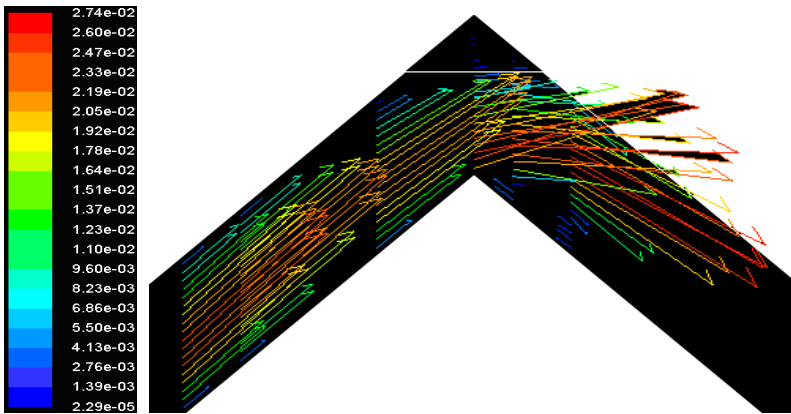
(b)

5.4 Pressure distribution

The pressure decrease with the distance from the entrance as expected, as shown in fig. 5.5. From the results obtained, it is seen that the pressure difference of the analysis increases with increase in the Reynolds number.

Figure 5.7Contours of static pressure at Re 3200: (a) wave design (b) chevron design

(a)

(b)

6. Conclusion

The heat transfer and pressure drop in plate heat exchangers, and it's dependency on geometry is reported in this study.

The heat transfer enhancement effect in corrugated plates is primarily due to induced turbulence which gives higher heat transfer rate.

From earlier definitions of the Nusselt number and friction factor, it is shown that the performance of a plate heat exchanger is dependent on the plate geometry (fig. 4.1 and 4.2). Since this is the case, the question now lies in 'the choice of suitable plate geometry'.

As shown from the study, different geometries give different results at different flow conditions (Reynolds number/ mass-flow rate). The choice of appropriate plate geometry does not always depend on high Nusselt number values, but predictability and almost constant behaviour through a large Reynolds number range, plays an important role as shown by the chevron design.

The choice of suitable plate geometry depends on the application. For example, for low Reynolds number applications, the wave design is shown to give better convective properties (approximately 22% more convective transfer), while at higher Reynolds numbers, the chevron design gives better convective properties (approximately 23% more convective transfer).

Appendices

Appendix A: Matlab script for laminar Reynolds number

```
clear all; close all; clc;
to=[335.80,328.74,344.62,337.28,329.48];
ti=[332.64,326.45,341.41,333.63,326.57];
[jj,kk]= size(to);
m=[0.05015,0.1003,0.2006,0.4012,0.8024];
v=[0.0061,0.0126,0.021,0.041,0.081];
dp=[0.07,0.15,0.95,2.60,7.33];
re=[100,200,400,800,1600];
tw=350;
cp=4182;
a=0.09426*2;
b=0.01;
d=2*b;
l=0.09426;
k=0.6;
de=998.2;
% x2=0.09;
% x1=0.03;
lmtd = zeros(jj,kk);
h = zeros(jj,kk);
nu = zeros(jj,kk);
f = zeros(jj,kk);

for cc = 1:kk
    dt=to(cc)-ti(cc);
    lmtd(cc)=((tw-ti(cc))-(tw-to(cc)))/log((tw-ti(cc))/(tw-to(cc)));
    h(cc)=(m(cc)*cp*dt)/(a*lmtd(cc));
    nu(cc)=h(cc)*d/k;
    f(cc)=(d*dp(cc))/(0.5*l*de*(v(cc))^2);
end

lmtd,h,nu,f

%chevy part
too=[339.19,332.94,339.95,331.63,325.45];
tii=[335.89,330.05,336.21,328.37,323.18];
[jjj,kkk]= size(too);
mm=[0.05015,0.1003,0.2006,0.4012,0.8024];
vv=[0.0092,0.0197,0.0294,0.058,0.12];
dpp=[0.16,0.44,2.15,6.03,18.11];
ree=[100,200,400,800,1600];
tw=350;
```

```matlab
cp=4182;
aa=0.1698;
bb=0.0071;
dd=2*bb;
ll=0.0848;
k=0.6;
de=998.2;
% x2=0.09;
% x1=0.03;
lmtdd = zeros(jjj,kkk);
hh = zeros(jjj,kkk);
nuu = zeros(jjj,kkk);
ff = zeros(jjj,kkk);

for ccc = 1:kkk
    dtt=too(ccc)-tii(ccc);
    lmtdd(ccc)=((tw-tii(ccc))-(tw-too(ccc)))/log((tw-tii(ccc))/(tw-too(ccc)));
    hh(ccc)=(mm(ccc)*cp*dtt)/(aa*lmtdd(ccc));
    nuu(ccc)=hh(ccc)*dd/k;
    ff(ccc)=(dd*dpp(ccc))/(0.5*ll*de*(vv(ccc))^2);
end

lmtdd,hh,nuu,ff

% pipe
tooo=[325.43,321.71,319.36,317.88,316.92];
tiii=[323.71,320.60,318.67,317.44,316.63];
[jjjj,kkkk]= size(tooo);
mmm=[0.05015,0.1003,0.2006,0.4012,0.8024];
vvv=[0.003,0.006,0.012,0.023,0.046];
dppp=[0.0045,0.0091,0.0188,0.0425,0.1087];
reee=[100,200,400,800,1600];
tw=350;
cp=4182;
aaa=0.12; %0.00377
ddd=0.02;
k=0.6;
de=998.2;
x2=0.09;
x1=0.03;
lmtddd = zeros(jjjj,kkkk);
hhh = zeros(jjjj,kkkk);
nuuu = zeros(jjjj,kkkk);
fff = zeros(jjjj,kkkk);

for cccc = 1:kkkk
    dttt=tooo(cccc)-tiii(cccc);
    lmtddd(cccc)=((tw-tiii(cccc))-(tw-tooo(cccc)))/log((tw-tiii(cccc))/(tw-tooo(cccc)));
```

```
    hhh(cccc)=(mmm(cccc)*cp*dttt)/(aaa*lmtddd(cccc));
    nuuu(cccc)=hhh(cccc)*ddd/k;
    fff(cccc)=(64/re(cccc));
end

lmtddd,hhh,nuuu,fff


figure(1)
plot(re,nu,'r')
xlabel('Reynolds number, Re')
ylabel('Nusselt number, Nu')
grid on
hold on
plot(re,nuu,'k')
hold on
plot(re,nuuu,'g')
legend('wave design','chevron design','straight pipe',2)
ginput

figure(2)
plot(re,f,'r')
xlabel('Reynolds number, Re')
ylabel('Friction factor, f')
grid on
hold on
plot(re,ff,'k')
hold on
plot(re,fff,'g')
legend('wave design','chevron design','straight pipe',1)

figure(3)
loglog(re,f,'r')
xlabel('Reynolds number, Re')
ylabel('Friction factor, f')
grid on
hold on
loglog(ree,ff,'k')
hold on
loglog(reee,fff,'g')
legend('wave design','chevron design','straight pipe',1)
```

Appendix B: Matlab script for turbulent Reynolds number

```
clear all; close all; clc;
to=[323.42,321.11,320.04,318.93];
ti=[321.55,319.30,318.60,317.98];
```

```matlab
[jj,kk]= size(to);
m=[1.6048,3.2096,6.4192,12.8384];
v=[0.162,0.325,0.655,1.324];
dp=[21.08,61.61,197.99,693.48];
re=[3200,6400,12800,25600];
tw=350;
cp=4182;
a=0.09426*2;
b=0.01;
d=2*b;
l=0.09426;
k=0.6;
de=998.2;
% x2=0.09;
% x1=0.03;
lmtd = zeros(jj,kk);
h = zeros(jj,kk);
nu = zeros(jj,kk);
f = zeros(jj,kk);

for cc = 1:kk
    dt=to(cc)-ti(cc);
    lmtd(cc)=((tw-ti(cc))-(tw-to(cc)))/log((tw-ti(cc))/(tw-to(cc)));
    h(cc)=(m(cc)*cp*dt)/(a*lmtd(cc));
    nu(cc)=h(cc)*d/k;
    f(cc)=(d*dp(cc))/(0.5*l*de*(v(cc))^2);
end

lmtd,h,nu,f

%chevy part
too=[323.14,322.13,321.55,321.13];
tii=[321.26,320.49,320.02,319.65];
[jjj,kkk]= size(too);
mm=[1.6048,3.2096,6.4192,12.8384];
vv=[0.256,0.517,1.045,2.09];
dpp=[67.81,258.60,1037.01,4120.16];
ree=[3200,6400,12800,25600];
tw=350;
cp=4182;
aa=0.1698;
bb=0.0071;
dd=2*bb;
ll=0.0848;
k=0.6;
de=998.2;
% x2=0.09;
% x1=0.03;
```

```matlab
lmtdd = zeros(jjj,kkk);
hh = zeros(jjj,kkk);
nuu = zeros(jjj,kkk);
ff = zeros(jjj,kkk);

for ccc = 1:kkk
    dtt=too(ccc)-tii(ccc);
    lmtdd(ccc)=((tw-tii(ccc))-(tw-too(ccc)))/log((tw-tii(ccc))/(tw-too(ccc)));
    hh(ccc)=(mm(ccc)*cp*dtt)/(aa*lmtdd(ccc));
    nuu(ccc)=hh(ccc)*dd/k;
    ff(ccc)=(dd*dpp(ccc))/(0.5*ll*de*(vv(ccc))^2);
end

lmtdd,hh,nuu,ff

% pipe
tooo=[317.74,316.41,315.83,315.86];
tiii=[317.07,316.07,315.59,315.66];
[jjjj,kkkk]= size(tooo);
mmm=[1.6048,3.2096,6.4192,12.8384];
vvv=[0.083,0.164,0.326,0.65];
dppp=[0.59,1.28,2.94,8.86];
reee=[3200,6400,12800,25600];
tw=350;
cp=4182;
aaa=0.12; %0.00377
ddd=0.02;
k=0.6;
de=998.2;
x2=0.09;
x1=0.03;
lmtddd = zeros(jjjj,kkkk);
hhh = zeros(jjjj,kkkk);
nuuu = zeros(jjjj,kkkk);
fff = zeros(jjjj,kkkk);

for cccc = 1:kkkk
    dttt=tooo(cccc)-tiii(cccc);
    lmtddd(cccc)=((tw-tiii(cccc))-(tw-tooo(cccc)))/log((tw-tiii(cccc))/(tw-tooo(cccc)));
    hhh(cccc)=(mmm(cccc)*cp*dttt)/(aaa*lmtddd(cccc));
    nuuu(cccc)=hhh(cccc)*ddd/k;
    fff(cccc)=(ddd*dppp(cccc))/(0.5*(x2-x1)*de*(vvv(cccc))^2);
end

lmtddd,hhh,nuuu,fff


figure(1)
```

```
plot(re,nu,'r')
xlabel('Reynolds number, Re')
ylabel('Nusselt number, Nu')
grid on
hold on
plot(ree,nuu,'k')
hold on
plot(reee,nuuu,'g')
legend('wave design','chevron design','straight pipe',2)
ginput

figure(2)
plot(re,f,'r')
xlabel('Reynolds number, Re')
ylabel('Friction factor, f')
grid on
hold on
plot(ree,ff,'k')
hold on
plot(reee,fff,'g')
legend('wave design','chevron design','straight pipe',1)

figure(3)
loglog(re,f,'r')
xlabel('Reynolds number, Re')
ylabel('Friction factor, f')
grid on
hold on
loglog(ree,ff,'k')
hold on
loglog(reee,fff,'g')
legend('wave design','chevron design','straight pipe',1)
```

References

1. www.thewcrgroup.com

2. **Jain, S.; Joshi, A.; Bansal, P. K.; 2007**
"A New approach to Numerical Simulation of Small Sized Plate Heat Exchangers With Chevron Plates"
Journal of Heat Transfer, Vol. 129, pp. 291-297

3. **Shah, R. K.; Focke, W. W.; 1988**
"Plate Heat Exchanger and Their Design Theory"
Hemisphere Washington, pp. 227-254

4. **Lee Y. S.; Sun Y.M.; Su C. C.; 2002**
"Experimental Study of Heat Transfer of Corrugated Channels"
First International Conference on Heat Transfer, fluid Mechanics, and Thermodynamics,
Kruger Park, South Africa

5. **Wilcox, D. C.; 2006**
"Turbulence Modeling for CFD"
DCW Industies, Inc., California, USA, ISBN 978-1-928729-08-2

6. **Kolmogorov, A. N.; 1942**
"Equations of Turbulent Motion of an Incompressible Fluid"
Izvestia Academy of Sciences, USSR
Physics, Vol. 6, No.1 and 2, pp. 56-58

7 **Chou, P. Y.; 1945**
"On the Velocity Correlations and the Solution of the Equations of Turbulent Fluctuation"
Quart. Appl. Math., Vol. 3, p. 38

8. **Rotta, J. C.; 1962**
"Turbulent Boundary layers in Incompressible Flow"
Progress in Aerospace Science, Vol. 2, p. 1

9. **Zeierman, S.; Wolfshtein, M.; 1986**
"Turbulent Time Scale for Turbulent Flow Calculations"
AIAA Journal, Vol. 24, No. 10, pp. 1606-1610

10. **Speziale, C. G.; 1998**
"Turbulence Modeling for Time-Dependent RANS and VLES: A Review"
AIAA Journal, Vol. 36, No. 2, pp. 173-184

11. **Fluent; 2003**
FLUENT 6.1 User's Manual

12. **Davidov, B. I.; 1961**
"On the Statistical Dynamics of an Incompressible Fluid"
Doklady Akademiya Nauk SSSR, Vol. 136, p. 47

13. **Harlow, F. H.; Nakayama, P. I.; 1968**
"Transport of Turbulent Energy Decay Rate"
Los Alamos Sci. Lab., University of California Report LA-3854

14. **Jones, W. P.; Launder, B. E.; 1972**
"The Prediction of Laminarization with a Two-Equation Model of Turbulence"
International Journal of Heat and Mass Transfer, Vol. 15, pp. 301-314

15. **Launder, B. E.; Sharma, B. I.; 1974**
"Application of the Energy Dissipation Model of Turbulence to the Calculation of Flow Near a Spinning Disc"
Letters in Heat and Mass Transfer, Vol. 1, No. 2, pp. 131-138

16. **Mansour, N. N.; Kim, J.; Moin, P.; 1988**
"Reynolds Stress and Dissipation Rate Budgets in Turbulent Channel Flow"
Journal of Fluid Mechanics, Vol. 194, pp. 15-44

17. **Morris, F. H.; Whitman, W. G.; 1928**
"Heat Transfer for Oils and Water in Pipes"
Industrial and Engineering Chemistry, Vol. 20, N0. 3

18. www.coolingzone/library.php?read=481

19. **Incropera, F. P.; DeWitt, D. P.; 1996**
"Introduction to Heat Transfer"
John Wiley & Sons, Inc, USA, ISBN 0-471-30458-1

20. http://ceeserver.cee.cornell.edu/mw24/cee331